Image-based Sorting and Negative Dielectrophoresis for High Purity Cell and Particle Separation

Journal:	*ELECTROPHORESIS*
Manuscript ID	elps.201800489.R3
Wiley - Manuscript type:	Research Paper
Date Submitted by the Author:	n/a
Complete List of Authors:	Thomas, Rupert; TTP Plc Mitchell, Peter; Adaptimmune Oreffo, Richard; University of Southampton, School of Medicine Morgan, Hywel; University of Southampton School of Electronics and Computer Science Green, Nicolas; University of Southampton, School of Electronics and Computer Science
Keywords:	Dielectrophoresis, Cell sorting, Image analysis, Particle separation, Virtual Channel

Image-based Sorting and Negative Dielectrophoresis for High Purity Cell and Particle Separation

Rupert S. W. Thomas [a], Peter D. Mitchell [b], Richard O.C Oreffo [b], Hywel Morgan [a,c] and Nicolas G. Green [*a]

a School of Electronics and Computer Science, University of Southampton Highfield, Southampton SO17 1BJ, UK. E-mail: ng2@ecs.soton.ac.uk.
b Bone and Joint Research Group, Centre for Human Development, Stem Cells and Regeneration, Human Development and Health, Institute of Developmental Sciences, Faculty of Medicine, University of Southampton, UK; E-mail: roco@soton.ac.uk
c Institute for Life Sciences, University of Southampton Highfield, Southampton SO17 1BJ, hm@ecs.soton.ac.uk

Video footage of device operation: https://goo.gl/FYMnyR

Abbreviations:

DEP	Dielectrophoresis
DVC	Dielectrophoretic Virtual Channels
FACS	Fluorescently Activated Cell Sorting
FCS	Fetal Calf Serum
HBMC	Human Bone Marrow Cells
MACS	Magnetically Activated Cell Sorting

Keywords:

Dielectrophoresis, Cell sorting, Image analysis, Particle separation, Virtual Channel

Abstract

Microelectrode arrays are used to sort single fluorescently labelled cells and particles as they flow through a microfluidic channel using dielectrophoresis (DEP). Negative DEP is used to create a "Dielectrophoretic Virtual Channel" (DVC) that runs along the centre of the microfluidic channel. By switching the polarity of the electrodes, the virtual channel can be dynamically reconfigured to direct particles along a different path. This is demonstrated by sorting particles into two microfluidic outlets, controlled by an automated system that interprets video data from a colour camera and makes complex sorting decisions based on colour, intensity, size and shape. This enables the rejection of particle aggregates and other impurities, and the system is optimised to isolate high purity populations from a heterogeneous sample. Green beads are isolated from an excess of red beads with 100% purity at a rate of up to 0.9 particles per second, in addition application to the sorting of osteosarcoma and human bone marrow cells is evidenced. The extension of DVCs to an arbitrary number of sorting outputs is examined, with design, simulation and experimental verification of two alternate geometries presented and compared.

1. Introduction

Biological cell populations typically occur in heterogeneous populations, with multiple specialised cell types in co-dependence. While the study of cells *in-vivo* is important, it can be difficult to determine the cause-effect relationships within such complex environments and the first step in many cell biology experiments is to isolate or purify the cells of interest. Fluorescently Activated Cell Sorting (FACS) has been widely adopted and involves the separation of individual particles into a stream of droplets which are charged and deflected by a high voltage applied between two deflection plates into a series of collection wells [1,2].

Although FACS machines have developed into sophisticated instruments capable of sorting many thousands of cells per second, they are typically large, expensive pieces of equipment which require considerable operator expertise. The method of operation (droplet jetting) can be unattractive and presents challenges around sample sterility and biosafety as a consequence of aerosol generation.

Microfluidics and dielectrophoresis may provide a useful alternative toolset: micro-scale channels and electrodes permit the manipulation and analysis of individual cells and particles. Multiple technologies need to reach maturity, however, before microfluidic cell and particle-based devices can become widespread – one of which is a means to reliably control the trajectory of particles [3]. The ability to specifically position particles is an enabling technology for sorting, but also permits biological and chemical reactions to be initiated or controlled by moving particles into different fluids, or via particle-particle interactions.

Particle position can be controlled either by manipulating the suspending fluid, or by exerting forces directly on the particles. Methods for manipulating the fluid include the use of electro-osmotic flow [4,5] and typically involve controlling the direction of fluid flow through a Y-shaped junction in a microfluidic channel. Although lacking the ability to manipulate individual cells, single cell resolution is achieved in practice by minimising the fluid volume within the junction and controlling the volumetric concentration of particles within the fluid. Dittrich et al. used this method for sorting beads, with output purities of 99.1% at 0.68 beads per second [5]. An alternative approach uses valves to control the fluid flow, which eliminates some variability associated with electrical flow control such as ion depletion within the suspending medium. Externally sited valves permit simple integration using standard components and has recently been combined with droplet encapsulation technology [6]. On-chip microvalves enable the construction of an integrated microfluidic device and minimises system dead volumes and have been demonstrated for cell sorting [7]. Methods for manipulating suspended particles directly include optical forces [8,9] and dielectrophoresis [10,11].

There is also much interest in cell isolation as a tool for medical therapeutic use. For example, mesenchymal or skeletal stem cells, which exist postnatally, are multipotent and can give rise to the stromal lineages (bone, cartilage, fat and myelosupportive stroma). Development of strategies for the isolation of skeletal stem cells could enable tissues for transplant to be grown *in vitro*, with a broad range of subsequent therapies for an ageing demographic. Skeletal stem cells can be obtained from bone marrow but are a minority subpopulation that comprises typically 0.01%-0.001% of mononuclear cells [12]. Efficiently isolating skeletal stem cells would significantly enhance therapeutic application [13]. Another example is autologous bone marrow transplants, in which a highly efficient method of separation is required to remove tumour cells from the graft product before it can be returned to the patient [14]. A wide range of laboratory techniques exist for the bulk separation of particles and biological cells - filtration, centrifugation, rosetting and magnetically activated cell sorting (MACS) to name just a few. In addition, the use of synthetic particles as chemical substrates, particularly for combinatorial chemistry, has opened another avenue of interest in sorting

applications. Bead-based (suspension) assays have received much interest as a means to significantly increase the number of simultaneously screened for targets, by using encoded microparticles to enable assay multiplexing [15,16]. This is particularly important in the field of DNA sequencing [17] and immunomagnetic particles have also been used to isolate very small numbers (<10) of circulating tumour cells (CTC) from millilitre quantities of blood as a diagnostic test for several key tumour types [18].

Sorting operations are active events, involving a decision – as opposed to separation, which occurs as a result of physical parameters such as size or electrical properties. Particle sorting requires inputs upon which to base decisions, for particle identification and/or differentiation. Photomultiplier tubes (PMT) are used in FACS machines to detect fluorescent labelling and/or scattered light, providing a light intensity measurement. Sensitive measurements can be made, but the sorting process is limited by the time taken to extrapolate the analogue waveform output. Label-free detection and sorting is an attractive alternative, not least because cells remain in an unaltered and unperturbed state [12]. Techniques include electrical impedance spectroscopy [19,20], deterministic lateral displacement [21,22] and real-time deformability cytometry [23].

Kovac and Voldman [9] demonstrated an alternative approach – image-based sorting, using a video camera. Multiple discrete measurements could be made on single cells immobilised in PDMS microwells, including sub-cellular spatio-temporal information. A significantly wider range of measurements can be extracted from video data than is available from a PMT; depending on the computational power available, complex feature extraction algorithms may be used to determine volume and morphology.

Image-based sorting can also be used for higher throughput devices. In this work, a colour video camera is used to detect cells and particles as they pass through a microfluidic channel, providing a rich set of measurements (size, intensity, colour, aggregation). This enables sorting decisions to be constructed around protocol objectives; here, purity of the sorted population is prioritised over throughput, and a protocol implemented to ensure particle aggregates are rejected. Dielectrophoresis (see below) is used to manipulate particles within the microfluidic channel, with the advantages of sterility and biosafety that are associated with working 'on-chip'. We demonstrate that cell and particle motion through the channel can be tightly controlled using 'virtual channels', and that these can be dynamically reconfigured as required.

2. Materials and Methods

2.1 Device Design: Dielectrophoresis

Dielectrophoresis (DEP) is the movement of polarisable particles caused by a spatially non-uniform electric field. Negative DEP (nDEP) is when cells are repelled from high-strength field regions at the edge of electrodes, while positive DEP describes the motion of cells toward those regions. Negative DEP is the preferred method of manipulating cells, since in physiological medium strong electric fields can induce cell damage. The theory of DEP is well covered in the literature and the equation for the time-averaged DEP force on a spherical particle is [24,25]:

$$\langle \mathbf{F}_{DEP} \rangle = \pi a^3 \varepsilon_m Re\left[\frac{\tilde{\varepsilon}_p - \tilde{\varepsilon}_m}{\tilde{\varepsilon}_p + 2\tilde{\varepsilon}_m}\right] \nabla |\mathbf{E}|^2 \quad (1)$$

where $\tilde{\varepsilon}_m$ and $\tilde{\varepsilon}_P$ are the complex permittivities of the suspending medium and the particle, a the particle radius, and $\mathbf{E}$ the peak value of the electric field. A discussion of the theory and device simulation is included in the electronic supplementary information (ESI).

Microfluidic devices have been fabricated with microelectrodes for DEP manipulation of single particles as they flow through the device, and in particular nDEP has been widely used to create barriers and for 2-dimensional confinement of particles into a focussed stream [19,26]. Planar electrodes on the top and bottom of the channel create a low field region in the centre of the channel towards which particles are directed under nDEP. If the DEP force is stronger than hydrodynamic drag, particles are confined to these low field regions. By shaping the electrode geometry so that low field regions are extruded along or at angles across the path of hydrodynamic flow, particles are carried through the microfluidic chip along trajectories that are defined and highly constrained only by the electric field. These are referred to here as Dielectrophoretic Virtual Channels (DVC), a complete discussion of which is in the ESI. This paper demonstrates how DVCs can be created and dynamically reconfigured to direct particles on a particular trajectory through a microfluidic device.

2.2 Device Fabrication

Microelectrodes were created using standard photolithographic techniques by deposition of platinum on to 700 µm thickness glass wafers. The wafers were designed with alignment marks on each chip so that the electrodes and channels could be aligned to within 5 µm. Matching pairs of metallised glass wafers were laminated with dry film resist (SY300 series, Elgar Europe), which was patterned to form the microfluidic features and aligned (EVG 620 TB double sided mask aligner) and bonded (EVG 520 TB) to together to form a sealed channel [27]. Microfluidic devices for particle sorting had channel dimensions of 200 x 25 µm (two x 20 µm thickness laminate layers, prior to bonding), and the height was increased to 40 µm for cell sorting (two x 30 µm thickness). Fluid channels for compound sorting gates were fabricated with dimensions of 1000 x 100 µm (two x 55 µm thickness). Individual chips were released from the bonded wafer pair by dicing, and holes for fluids made using a mechanical drill. Figure 1A and B show an overview of a microfluidic device, and an enlarged view of the channel and electrodes.

2.3 Device Operation

Figure 1C shows the concept of an image-based DVC sorting gate operating at a microfluidic junction. The electrodes located at the junction exert a DEP force on the particles as they are carried through by the fluid flow. Particles are first focussed into a narrow stream by the two pairs of large opposing electrodes (focussing electrodes), as they move along the channel in a DVC that runs through the centre of the group of electrodes. A third pair of opposing electrodes (the sorting electrodes) directs the DVC towards either of the fluid outlets. An automated control system switches the polarity of the sorting electrodes to direct particles towards the required fluid outlet, shown schematically using red and green particles. In addition to the electrodes for the particle focussing and the sorting gate, the device incorporated additional electrodes (visible in the centre of the device, Figure 1B) for impedance spectroscopy that were not used in this work.

2.4 Optical System

A custom-built microscope was built around a uEye 2230c colour video camera and a Nikon 4x objective lens. Simultaneous FITC/CY5 fluorescence observations were possible using a dual band polychroic mirror and emission filter (Chroma, Laser 2000), with illumination from 473 and 635 nm lasers (Laserglow).

2.5 Fluidic Interfacing

Microfluidic devices were clamped within a fluid manifold with four inlets and outlets, each with a manual on/off valve (Omnifit). One of these inlets was connected to a syringe pump that was used to

flow the sorting buffer throughout the fluidic system, the other three being connected to air-tight fluid reservoirs through separate channels of a Flowel flow measurement unit (Fluigent). Fluid flow from each of the reservoirs was controlled by gas pressure in the range of 0-25 mbar by a MFCS-4C flow control system (Fluigent).

2.6 Electronic Systems and Software Control

The sorting electrodes were energised with a sinusoidal voltage of 12 Vpp at 1 MHz from a function generator, switched through RF switches (Panasonic AQY221N2S) and interfaced to a computer through a National Instruments USB-6501 digital I/O device. Electrical interconnection was provided to the glass microfluidic device by spring contacts on two printed circuit boards built into the fluid manifold. Custom software, written in MATLAB (Mathworks, MA) provided real-time video frame analysis, recording, and electrode control. Steps in processing the video frames included: removing static features by subtracting a stored background image, thresholding on intensity to create a binary image, identifying continuous regions in the image, and filtering by region size, colour (hue in HSV space), and shape (eccentricity). Further discussion and parameters may be found in the ESI.

2.7 Fluorescent Particles

Fluorescent polystyrene microparticles (Bangs Laboratories) were suspended in a neutrally buoyant (to minimise settling and particle-particle interactions) sorting buffer (0.02% TWEEN-20, 0.1% PBS, 12.8% sucrose in aqueous suspension), conductivity $\sigma_m = 0.18\ Sm^{-1}$ at a concentration of 10^6 ml^{-1}. Red and green particles (5.5 µm diameter) were mixed to create a heterogeneous population with a ratio of approximately 10:1 for sorting (final ratio 91.5:8.5 measured by FACS), and green particles (15.6 µm diameter) were used unmixed with the compound sorting gates.

2.8 Biological particles

Immortalized human MG-63 cells (osteosarcoma—ATCC, CRL-1427) were established as monolayer cultures in Dulbecco's Modified Eagle Medium (DMEM) plus 10% fetal calf serum (FCS). Cells were maintained at 37°C with 5% CO_2 and passaged at preconfluence for maintenance or use in experiments. Freshly isolated bone marrow samples were obtained from haematologically normal osteoarthritic patients undergoing routine total hip replacement surgery with approval of the Southampton & South West Hampshire Local Research Ethics Committee (LREC194/99). Samples were suspended in αMEM + 10% FCS, Penicillin (100U/mL) and Streptomycin (0.1mg/mL) and centrifuged to remove fat. Bone fragments and blood clots were sieved out prior to removal of red blood cells via centrifugation for 40 minutes at 2200 rpm, 18°C using LymphoPrep™. Isolated cells were washed with phosphate buffered saline (PBS), plated and cultured in αMEM + 10% FCS at 37°C, 5% CO_2.

MG-63 cells and human bone marrow cells (HBMCs) were dissociated from tissue culture plastic using Accutase (Invitrogen), and labelled using a two-step immunostaining protocol for STRO-1. Anti-STRO-1 primary antibody was applied, followed by an Alexa-Fluor 488-conjugated secondary antibody, used to provide fluorescent marking of STRO-1 positive cells. A non-discriminating cell label - Vybrant DiD (Molecular Probes) - was applied to cells post-immunostaining to counterstain all cells red to enable the clear observation of cells within the microfluidic device. In ideal circumstances target and non-target cells would be each labelled with a different fluorescent antibody, but this remains a significant challenge as the populations contain a range of cell types each with varying degrees of expression of an unknown range of antigens. Cells were resuspended in a sort buffer (PBS + 1% BSA, 5mM EDTA, 25 mM HEPES, 12.8% Dextran-50), conductivity $\sigma_m = 1.6 Sm^{-1}$ at a concentration of 10^6 ml^{-1} before use.

3 Results

3.1 Sorting at a microfluidic junction

Sorting performance was analysed through video and confirmed by flow cytometry analysis of sorted and waste populations from the device. Fluorescently labelled green particles were isolated (Figure 2A) from a heterogeneous population (majority red particles) using a conservatively skewed sorting strategy intended to maximise the purity of the green sorted population, as detailed below. Figure 2B shows a plot of the results of a number of sorting operations, as the fluid volumetric flow rate was controlled between 20 and 100 nl min^{-1}.

The contents of the sorted sample were manually counted under a fluorescence microscope following recovery from the microfluidic system and the green fraction determined – a value of 1.0 representing a pure green sample. The waste sample was counted by automated analysis on a FACS machine (BD FACSAria). The experimental data is summarised in Table 1, with running time and sorting rate for each operation.

Sorted samples were 100% pure (composed entirely of the green particles) when sorted at flow rates of up to 60 nl min^{-1}. The purity of the sorted population declined as the flow rate was increased, as the decision time of the control software was unable to match the rate of particles entering the active region. A 'delay compensation' scheme was introduced by offsetting the detection region forward of the active region (by approximately 25 µm upstream, determined empirically), thereby improving the purity at higher flow rates – the red line in Figure 2B.

The maximum flow rate (100 nl min^{-1}) was the maximum at which particles could be reliably deflected with the configuration used (particle size, and electrode voltage and spacing). As Equation 1 shows, revision of these parameters could increase this limit. The maximum flow rate at which pure populations were achieved (60 nl min^{-1}) corresponded to a sorting rate of 0.89 particles per second.

3.2 Image-based sorting

Real-time image acquisition and processing scripts were constructed in MATLAB (Mathworks) as an automated control system for image-based sorting. This enabled decision algorithms to operate on video data, and identify particles by colour, intensity, size and geometric features. Figure 2A shows a screenshot of the system in operation, and a sequence of images showing stages in the image analysis process. Motion blur caused elongation of the particle image, a function of the exposure time of the camera. This reduced the degree to which the particle position could be localised. Enlargement of the detection region compensated for this but could reduce the collection yield if the bead population was concentrated and the particle spatial separation correspondingly low. A frame rate of 10 fps was used as this was the computational limit imposed by the hardware/software combination, however, higher speeds would be possible if a lower level language were used.

3.3 Optimised sorting strategies

Although a straightforward sorting strategy for a mixed population would be to direct one species of particle towards each outlet, it may be more appropriate to adopt a strategy that is optimised towards a relevant sorting priority. Example strategies could aim to maximise purity, sorting rate, or number of particles recovered, with a trade-off usually existing between parameters.

In the manipulation of biological cells, a typical application is rare cell isolation. This favours a sorting strategy that optimises the purity of the target population, providing the target species comprises a sufficiently large fraction of the total population.

Green fluorescent beads were designated as 'target' particles and formed a minority (8.5%) within the red/green population. A sorting strategy was developed to isolate the green beads from the heterogeneous population at the highest possible purity, at the expense of sorting rate and the numbers of particles recovered. Of the two outlets from the microfluidic Y-junction, one was designated a 'waste' output through which all particles (target and non-target) were directed by default. Additionally, the fluid flow through the junction was skewed (using reservoir gas pressure) so that the majority (60%/40%) left through the waste output. The other output was designated the 'collection' output and target particles were only directed towards it if it was expected that they could be recovered without contamination, under conditions: the presence of any non-target particles shortly before or after a target particle should trigger both particles to be directed to waste; and particles above a certain size threshold should be directed to waste, as aggregates of several particles may conceal a non-target particle. As evidenced in Table 1, the green fraction in the waste sample showed approximate correlation with the sorting rate, indicating that the proportion of target particles recovered was reduced at higher sorting rates.

Image-based sorting permits multiple particles to be distinguished simultaneously, which is most advantageous when conducting high-purity sorting of real-world populations, as particle aggregations and variations in size and intensity complicate particle identification.

3.4 Sorting fluorescently-labelled human cells

A significantly greater challenge is the isolation of specific human cells from a heterogeneous population. A successful platform requires robust methods of cell identification and manipulation, tolerant to variations in size, morphology and particle aggregations, with consideration to cell health and viability including management of temperature, nutrition and micro-environment. An example is the enrichment or ideally purification of skeletal stem cells from human bone marrow, via previously identified cell surface markers such as STRO-1 which is indicative, although it should be noted not exclusively for such cells [13].

Microfluidic devices with channels of depth 40 µm were used to sort cells, minimizing exposure to shear flow close to the channel walls. Electrode excitation of 5 Vpp at 5 MHz was used – the reduction in voltage and increase in frequency both reducing the induced transmembrane potentials [28]. The fluid flow rate was reduced to 20 nl min^{-1} to compensate for the reduction in DEP force. Figure 2C shows two photographs of HBMCs during sorting operations – the background illumination (white light) has been removed to improve contrast and the blue laser (exciting green fluorescence) is reduced to a spot 100 µm in diameter over the detection region. Target cells (labelled with STRO-1 and Alexa-Fluor 488 fluorescent antibody) were directed to the collection outlet. All other particles were directed to the waste. The figure also shows the common problem of target/non-target aggregations that complicate particle identification.

Sorted cells were recovered by flushing the device with clean sort buffer into a single well of a 96-well plate. An equal volume of PBS was added, and the plate centrifuged to allow resuspension of the cells in pre-conditioned culture media (recovered from the flasks used to maintain the cells while in culture) plus 20% FCS and 1% penicillin/streptomycin.

A summary of experimental data from the sorting of human cells from 10 consecutive sorting operations is presented in Table 2. A mean sorting rate of 0.24 cells per second was achieved, based

on the sorting of (approximately) 5020 cells. This is likely to be a lower estimate as the automated count may not fully identify all the cells within cell aggregations. Sorted and recovered cell populations contained 100% STRO-1 labelled cells, identified by visual inspection of the microplates using a fluorescence microscope one hour after sorting. Control samples were taken from each of the prepared and labelled cell populations prior to sorting and did not pass through the microfluidic cell sorter. These samples were added to the 96-well plate and cultured in the same manner as the sorted population.

The proportion of sorted target cells recovered from the device was consistently lower than anticipated, averaging 73.9%. The exact mechanism for this reduction is unclear but may be due to cells attaching to surfaces within the system and subsequent retention during flushing. Viability of sorted and control populations was assessed seven days after return to culture, by manual inspection on an inverted microscope to determine cell adherence and proliferation. Cell viability was observed to be consistently lower (-16.3%) than control samples, and more so for HBMCs (-20.8%) than MG63 cells (-9.7%). The sorting process places cells under electrical, thermal and fluidic stresses, and it is likely an established osteosarcoma cell line may withstand this better than primary cells. Exploration of the relative significance of these factors should be considered in future work.

3.5 Multiple-channel sorting using reconfigurable virtual channels

Sorting gates can be stacked, so that the output of one feeds into the input of the next, and a single stream of particles can be sorted into (n+1) outputs by n gates. This is inefficient in terms of substrate area and the number of electrical connections required. It is possible to merge a set of gates into a single group of electrodes with multiple outputs, with a corresponding reduction in the required number of electrical connections and substrate area. This enables multiple sub-populations to be simultaneously isolated from a heterogeneous sample.

Two designs of compound sorting gates were constructed using multi-layer electrodes. The operation of the two designs (A and B) of compound sorting gate are shown in Figure 3A and B. Design A is the equivalent of four single sorting gates stacked and merged together with five spatially separated output paths. Design B is a development of Design A, with more accurately defined paths through the sorter and a greater magnitude of separation between the output streams. One electrode is shared between all the stages of the sorting junction (in both designs), with the last electrode of each stage forming the first electrode of the next stage. A complete discussion of the electrode configuration, simulation and operation of the two designs can be found in the ESI.

Figure 3A(i) and B(i) shows a sequence of images as 15 µm polystyrene particles were directed through the outputs of the sorting gates. Custom particle-image velocimetry software (written in MATLAB) was used to produce the superimposed plot of the bead trajectories through gates – Figure 3A(ii) and B(ii). An image of the electrodes and channel wall is superimposed, with the top metal layer (from which the DEP force originates) coloured in solid black.

Numerical simulation of the electric field was performed using FlexPDE™ software and contour plots of the electric field were produced using the VisIT Visualisation Tool™. An example of one configuration of electrode polarity is shown for each design – Figure 3A(iii) and B(iii) - demonstrating the creation of a DVC through one sorting gate. A complete discussion of the results of numerical simulation and all configurations can be found in the accompanying ESI. Comparison with the experimental results shows the particle trajectories follow the plotted low field regions.

The width of and separation between the output streams were measured 70 µm from the exit of the sorter. Design B was designed to direct particles along the centre-line of the outlet, so the offset from

this ideal path was also measured. These measurements are presented in Table 2. Output streams from Design B were more focussed, and more separated, than the outputs of Design A. This would reduce errors occurring between particles leaving the sorting gate and entering a subsequent processing stage. Design B is scalable in terms of increasing separation distance, provided the angle between the electrode leading edge and the fluid flow is not significantly increased. The centre offset measured for Design B is due to asymmetry in the electrode geometry around the outlet and could be improved by extending the electrode outlet.

4. Discussion

Negative dielectrophoretic sorting gate electrodes have been shown to be suitable for isolation of single particles with high purity. Minority sub-populations of fluorescent beads have been enriched from 8.5% to 100% purity, at rates of up to 0.9 particles per second (60 nl min^{-1} flow rate).

The use of electrodes and the action of nDEP have been used to create 'tunnels' along microfluidic channels – Dielectrophoretic Virtual Channels. Particles were carried along this channel by Stokes drag from the suspending fluid and held in by the action of nDEP. Electrode voltages of 12 Vpp were used (±6 V around a fixed ground), with an electrode spacing of 20 µm (5 Vpp and 40 µm for work with biological cells). The DEP force could be increased (and hence a potential increased maximum sorting rate) in proportion to the square of the field strength, so could be significantly increased by a reduction in the electrode spacing or increase in voltage.

Image-based particle sorting has been shown to be a practical method for sorting fluorescent particles at relatively low rates, of around one particle per second. The method is advantageous as it negates some of the requirement for the more advanced optical equipment required in many sorting devices, such as photomultiplier tubes, and lessens the required alignment tolerances of the optical system. The device used in this work could also be operated on a standard fluorescence microscope. The use of image-based sorting (rather than threshold detection, as commonly used in commercial FACS machines) allows sophisticated decision algorithms to be used to distinguish 'target' from 'non-target' particles, incorporating factors such as particle size, shape or colour by simple changes to the control software.

The extension of the simple sorter to compound sorting gates was also demonstrated. Of the two designs demonstrated, Design B was a development that confined particles to narrow streams along clearly defined trajectories – with stream widths measured at less than 10 µm. This could be improved further, with a redesign of the electrodes. The ability to precisely move and position particles within a microfluidic device is an enabling technology for the wider adoption of particle-based devices. Of particular interest is their use to sort cells, and while microfluidic devices are unlikely to approach the throughput of their larger-scale counterparts, they are of utility for integrated cell-based devices and analysis platforms.

Acknowledgements

The authors would like to acknowledge the assistance of Katie Chamberlain for fabrication of the microfluidic devices.

References

[1] Eisenstein, M., Nature, 2006, 441, 11791185.
[2] Herzenberg, L. A., Sweet, R. G., Herzenberg, L. A., Sci. Am., 1976, 234, 108-117.
[3] Derveaux, S., Stubbe, B. G., Braeckmans, K., Roelant, C., Sato, K., Demeester, J., De Smedt, S. C., Anal. Bioanal. Chem., 2008, 391, 2453–2467.
[4] Fu, A. Y., Spence, C., Scherer, A., Arnold, F. H., Quake, S. R., Nat. Biotechnol., 1999, 17, 1109-1111.
[5] Dittrich, P. S., Schwille, P., Anal. Chem., 2003, 75, 5767-5774.
[6] Cao, Z., Chen, F., Bao, N., He, H., Xu, P., Jana, S., Jung, S., Lian, H., Lu, C., Lab Chip, 2013, 13, 171-178.
[7] Fu, A. Y., Chou, H. P., Spence, C., Arnold, F. H., Quake, S. R., Anal. Chem., 2002, 74, 2451-2457.
[8] MacDonald, M. P., Spalding, G. C., Dholakia, K., Nature, 2003, 426, 421-424.
[9] Kovac, J.R., Voldman, J., Anal. Chem. , 2007, 79, 932130.
[10] Baret, J., Miller, O. J., Taly, V., Ryckelynck, M., El-Harrak, A., Frenz, L., Rick, C., Samuels, M. L., Hutchison, J., Agresti, J. J., Link, D. R., Weitz, D. A., Griffiths, A. D., Lab Chip, 2009, 9, 1850-1858.
[11] Thomas, R. S. W., Mitchell, P. D., Oreffo, R. O. C., Morgan, H., Biomicrofluidics, 2010, 4, 022806.
[12] Xavier, M., Oreffo, R. O. C., Morgan, H., Biotechnol. Adv., 2016, 34, 908-923.
[13] Gothard, D., Tare, R. S., Mitchell, P. D., Dawson, J. L., Oreffo, R. O. C., Lab Chip, 2012, 11, 1206-1120.
[14] Dainiak, M. B., Kumar, A., Galaev, I. Y., Mattiasson, B., Adv. Biochem. Eng. Biot., 2007, 106, 1-18.
[15] Derveaux, S., De Geest, B. G., Roelant, C., Braeckmans, K., Demeester, J., De Smedt, S. C., Langmuir, 2007, 23, 10272-10279.
[16] Birtwell, S., Morgan, H., Integr. Biol., 2009, 1, 345-362.
[17] Zhi, Z., Morita, Y., Yamamura, S., Tamiya, E., Chem. Commun., 2005, 2448-2450.
[18] Toonder, J., Lab Chip, 2011, 11, 375-377.
[19] Gawad, S., Schild, L., Renaud, P., Lab Chip, 2001, 1, 76-82.
[20] Sun, T., Holmes, D., Gawad, S., Green, N. G., Morgan, H., Lab Chip, 2007, 7, 1034-1040.
[21] Huang, L. R., Cox, E. C., Austin, R. H., Sturm. J. C., Science, 2004, 304, 987–990.
[22] McGrath, J., Jimenez, M., Bridle, H., Lab Chip, 2014, 14, 4139–4158.
[23] Otto, O., Rosendahl, P., Mietke, A., Golfier, S., Herold, C., Klaue, D., Girardo, S., Pagliara, S., Ekpenyong, A., Jacobi, A., Wobus, M., Töpfner, N., Keyser, U. F., Mansfeld, J., FischerFriedrich, E., Guck, J., Nat. Methods, 2015, 12, 199–202.
[24] Jones, T. B., AC Electromechanics of Particles, Cambridge University Press, Cambridge, 1995.
[25] Morgan, H., Green, N. G., AC Electrokinetics: colloids and nanoparticles, Research Studies Press, Baldock, 2003.
[26] Holmes, D., Morgan, H., Green, N. G., Biosens. Bioelectron. , 2006, 21, 1621-1630.
[27] Vulto, P., Glade, N., Altomare, L., Bablet, J., Tin, L. D., Medoro, G., Chartier, I., Manaresi, N., Tartagni, M., Guerrieri, R., Lab Chip, 2005, 5, 158-162.
[28] Kotnik, T., Bobanovic, F., Miklavcic, D., Bioelectrochem. Bioenerg. , 1997, 43, 285-291.

Figure Legends

Fig. 1 (A) Photograph of the microfluidic device and electrodes (black), and an enlarged view of the microfluidic channel area (B). The microfluidic inlets/outlets are numbered, 1: cell suspension inlet, 2: sorted cells outlet, 3: waste outlet, 4: plain sort buffer inlet (without cells). (C) Concept diagram of the dielectrophoretic sorting gate at a microfluidic junction. The blue contour plot shows the shape of the region of low electric field strength (the negative DEP Virtual Channel) created between the electrodes. Particles suspended in the fluid are carried through the junction with the DEP force confining the particles to the DVC which can be directed towards either outlet. In the enlargement, the polarity of the sorting electrodes is reversed, showing the alternate DVC route.

Fig. 2 (A) Results of automated sorting of mixtures of red/green fluorescent beads with a screen image of the sorting software during operation. The detection region has been overlaid as a dashed white box. Image processing algorithms compare a stored 'background' image (i) to the current video frame (ii) using an absolute difference function on the relative intensities of each pixel. The resultant intensity map (iii) is converted to a binary image (iv) using a threshold function, and continuous regions identified by detecting interconnecting pixels. (B) Plot of sorted fraction versus flow rate with pure green populations achieved at up to 60 nl min^{-1}, at a rate of 0.9 beads/sec. (C) Fluorescently labelled human bone marrow cells (HBMCs) during sorting: (i) target cell directed toward the collection outlet, and (ii) a non-target cell and cell aggregate directed toward the waste outlet.

Fig. 3 Operation of the compound sorting gates (Design A above, Design B below) with 15µm fluorescent particles. A(i) and B(i) show video still images of particles passing through each of the outputs (5 for design A and 4 for design B). A(ii) and (Bii) show composite particle trajectories as they pass through each of the outputs, with each dot represents a single particle in a single frame of the video data (recorded at 40 fps, flow rate of 1 µl min^{-1}, electrode voltage 12 Vpp, 1 MHz). A(iii) and B(iii) show numerical simulation of the electric field (contour plot of the low field region) with the sorter configured to direct particles through one of the outlets – note the reversed electrode polarity (red and black). Further simulation plots can be found in the ESI.

Table 1 (A) Results of automated sorting of mixtures of red/green fluorescent beads at various flow rates and (B) results of sorting STRO-1 labelled human cells, all at 20 nl min^{-1} flow rate.

Table 2 Measurements of the particle streams from each of the outputs of Design A and B.

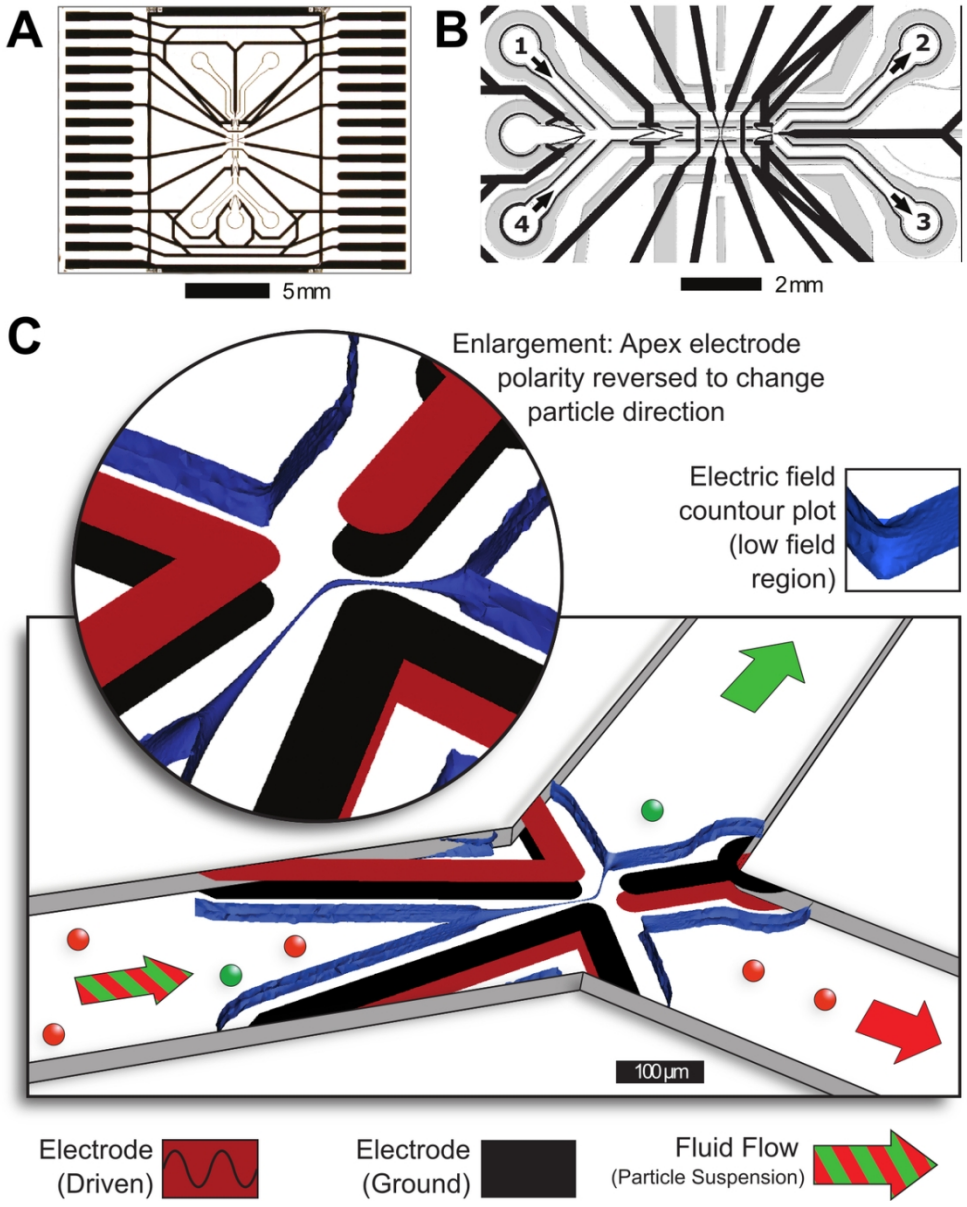

Fig. 1 (A) Photograph of the microfluidic device and electrodes (black), and an enlarged view of the microfluidic channel area (B). The microfluidic inlets/outlets are numbered, 1: cell suspension inlet, 2: sorted cells outlet, 3: waste outlet, 4: plain sort buffer inlet (without cells). (C) Concept diagram of the dielectrophoretic sorting gate at a microfluidic junction. The blue contour plot shows the shape of the region of low electric field strength (the negative DEP Virtual Channel) created between the electrodes. Particles suspended in the fluid are carried through the junction with the DEP force confining the particles to the DVC which can be directed towards either outlet. In the enlargement, the polarity of the sorting electrodes is reversed, showing the alternate DVC route.

102x124mm (300 x 300 DPI)

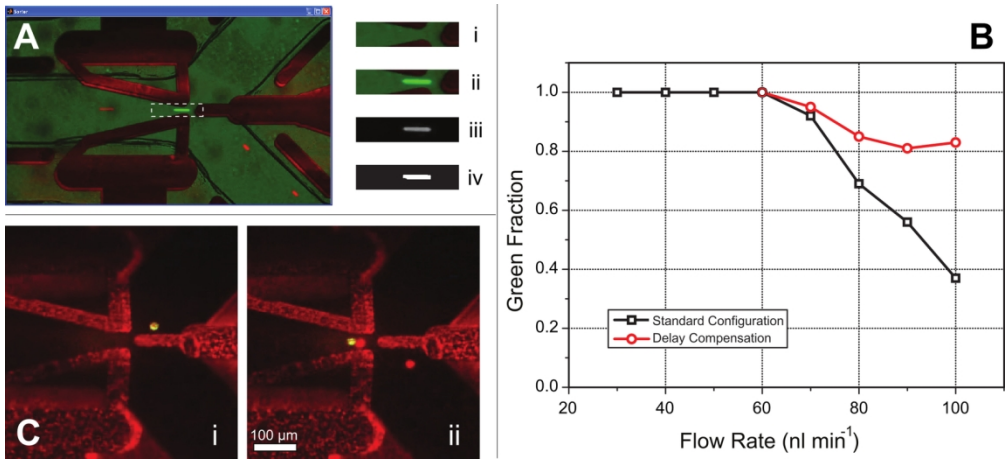

Fig. 2 (A) Results of automated sorting of mixtures of red/green fluorescent beads with a screen image of the sorting software during operation. The detection region has been overlaid as a dashed white box. Image processing algorithms compare a stored 'background' image (i) to the current video frame (ii) using an absolute difference function on the relative intensities of each pixel. The resultant intensity map (iii) is converted to a binary image (iv) using a threshold function, and continuous regions identified by detecting interconnecting pixels. (B) Plot of sorted fraction versus flow rate with pure green populations achieved at up to 60 nl min-1, at a rate of 0.9 beads/sec. (C) Fluorescently labelled human bone marrow cells (HBMCs) during sorting: (i) target cell directed toward the collection outlet, and (ii) a non-target cell and cell aggregate directed toward the waste outlet.

148x67mm (300 x 300 DPI)

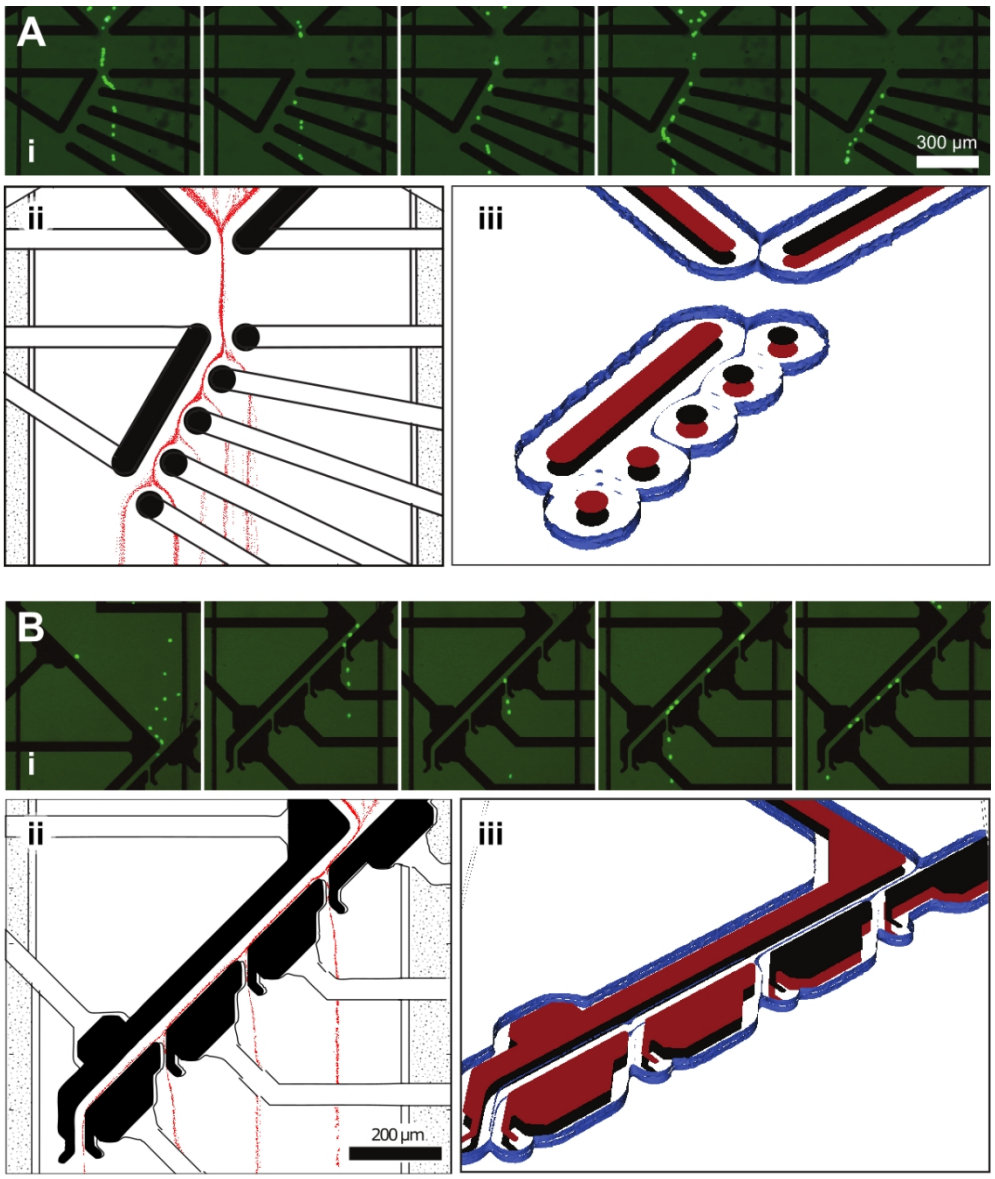

Fig. 3 Operation of the compound sorting gates (Design A above, Design B below) with 15µm fluorescent particles. A(i) and B(i) show video still images of particles passing through each of the outputs (5 for design A and 4 for design B). A(ii) and (Bii) show composite particle trajectories as they pass through each of the outputs, with each dot represents a single particle in a single frame of the video data (recorded at 40 fps, flow rate of 1 µl min-1, electrode voltage 12 Vpp, 1 MHz). A(iii) and B(iii) show numerical simulation of the electric field (contour plot of the low field region) with the sorter configured to direct particles through one of the outlets – note the reversed electrode polarity (red and black). Further simulation plots can be found in the ESI.

153x186mm (200 x 200 DPI)

Red/Green Fluorescent Particles									
Flow Rate	**Collection Sample**		**Green Fraction**			**Total**	**Run Time**	**Sorting rate**
(nl min^{-1})	**Red**	**Green**	**Input**	**Waste**	**Collection**	**Particles**	(mm:ss)	(sec^{-1})
standard configuration:								
30	0	38	0.085	0.011	1.000	506	28:07	0.30
40	0	46	0.085	0.020	1.000	694	27:32	0.42
50	0	59	0.085	0.006	1.000	741	22:52	0.54
60	0	75	0.085	0.022	1.000	1165	21:49	0.89
70	9	95	0.085	0.016	0.913	1353	29:40	0.76
80	27	59	0.085	0.028	0.686	1000	32:49	0.51
90	86	107	0.085	0.041	0.554	2271	31:44	1.19
100	139	82	0.085	0.050	0.371	2024	23:35	1.43
with delay compensation:								
60	0	66	0.085	0.013	1.000	906	22:32	0.67
70	4	81	0.085	0.020	0.953	1224	25:11	0.81
80	19	99	0.085	0.019	0.839	1471	23:08	1.06
90	44	192	0.085	0.016	0.814	2718	23:58	1.89
100	29	138	0.085	0.025	0.826	2248	22:02	1.70

Biological Cells

Run Number	Target Cells Sorted	Cells Recovered	Target Cells Recovered	Purity (%)	Control Viability (%)	Sorted Viability (%)	Proliferation Observed	Total Cells Sorted (approx.)	Run Time (approx.) (min)	Sorting Rate (cells/sec)
Cell Type/Source MG-63 (culture)										
1	35	24	24	100.0%	75.2	54.2	Yes	515	30	0.29
2	25	17	17	100.0%	71.7	70.6	Yes	417	30	0.23
3	20	12	12	100.0%	65.5	58.3	Yes	357	30	0.20
4	25	19	19	100.0%	72.6	63.2	Yes	417	30	0.23
Cell Type/Source HBMC (F81)										
5	15	9	9	100.0%	47.9	11.1	Yes	385	30	0.21
6	20	17	17	100.0%	44.8	41.1	Yes	556	30	0.31
7	20	16	16	100.0%	44.8	12.5	Yes	513	30	0.28
8	30	20	20	100.0%	37.9	25.0	Yes	714	45	0.26
9	30	26	26	100.0%	37.9	19.2	Yes	667	45	0.25
10	10	10	10	100.0%	30.1	10.0	Yes	481	45	0.18

Design A					
Outlet:	**1**	**2**	**3**	**4**	**5**
Stream Width (μm)	16	11	10	17	24
Stream Separation (μm)	**1 – 2**	**2 – 3**	**3 – 4**	**4 – 5**	
	96	47	46	41	

Design B				
Outlet:	**1**	**2**	**3**	**4**
Stream Width (μm)	4	7	4	5
Centre Offset (μm)	4.5	12	11	12
Stream Separation (μm)	**1 – 2**	**2 – 3**	**3 – 4**	
	170	147	146	